TECHNICAL ARTICLE

Effect of Co substitution on the martensitic transformation and magnetocaloric properties of $Ni_{50}Mn_{35-x}Co_xSn_{15}$

F.S. Liu, Q.B. Wang, S.P. Li, W.Q. Ao, and J.Q. Li[a]
College of Materials Science and Engineering, Shenzhen University and Shenzhen Key Laboratory of Special Functional Materials, Shenzhen 518060, China

Martensitic transformation and magnetic entropy change in Co substituted $Ni_{50}Mn_{35-x}Co_xSn_{15}$ ($x = 0$, 1.0, 1.5, 2.0, and 3.0) Heusler alloys have been investigated by X-ray powder diffraction analysis, differential scanning calorimetry, and magnetic measurements. X-ray diffraction analysis reveals that the $Ni_{50}Mn_{35-x}Co_xSn_{15}$ alloys have $L2_1$ Heusler structure at room temperature. The phase decomposition of the sample with $x = 3.0$, after annealing 48 h at 1173 K, is confirmed by both X-ray powder diffraction analysis and energy-dispersive x-ray spectroscopy in scanning electron microscopy. With the increase of the Co content from 0 to 2.0, the martensitic transformation temperature T_M increases from 185 to 245 K, which is in good agreement with the rule of valence electron concentration e/a-dependence of T_M. The magnetic entropy change ΔS_M is investigated in the vicinity of the martensitic transformation. © 2013 International Centre for Diffraction Data. [doi:10.1017/S0885715613000225]

Key words: Heusler alloys, martensitic transformation, magnetocaloric effect

I. INTRODUCTION

Owing to its promising potential on energy saving and environmental safety, much attention has been focused on magnetic refrigeration, which is considered as an alternative to the conventional gas-based refrigeration technique. Magnetic refrigeration is based on the magnetocaloric effect (MCE) described in terms of isothermal magnetic entropy change (ΔS_M) and/or adiabatic temperature change (ΔT_{ad}). A variety of prototype materials and intermetallic compounds have been studied in order to achieve a large MCE at proper temperatures. Since the discovery of giant MCE in $Gd_5(Ge_{1-x}Si_x)_4$ alloys (Pecharsky and Gschneidner, 1997), which undergo a first order magnetic transition coupled with the crystal structural transition, many other compounds with giant MCE have been found, such as La–Ca–Sr–Mn–O manganites (Zhang et al., 1996), MnAs (Kuhrt et al., 1985), $MnFeP_{1-x}As_x$ (Tegus et al., 2002), $MnAs_{1-x}Sb_x$ (Wada and Tanabe, 2001), $LaFe_{13-x}Si_x$ (Hu et al., 2001), MnNiGe (Zhang et al., 2008), MnCoGe, etc. Among these materials, Ni–Mn-based ferromagnetic shape memory alloys (FSMAs) Ni–Mn–Z (Z = Ga, In, Sn, and Sb) have received increasing attention because of several noteworthy characteristics such as large magnetic field-induced-strain (Kainuma et al., 2006), relatively cheap raw materials, and adjustable phase transition temperature (Krenke et al., 2005a). High MCE with $|\Delta S_M|$ of 86 J kg^{-1} K^{-1} in a field change of 50 kOe at about 313 K has been reported in a Ni_2MnGa single crystal (Pasquale et al., 2005). A large magnetic entropy change ΔS_M of 19 J kg^{-1} K^{-1} in a field change of 50 kOe in $Ni_{50}Mn_{50-x}Sn_x$ alloys is obtained near its martensitic transformation (MT) at 300 K (Krenke et al., 2005a). A large MCE has been observed due to the sudden increase of magnetization (ΔM) by the magneto-structural transition from the martensitic phase to the austenitic phase in the Ni–Mn–Z system.

It was reported that there is a ferromagnetic (FM) coupling between the Mn atoms while the magnetic moments of the Ni atoms were kept zero in the stoichiometric Ni_2MnZ alloys (Helmholdt and Buschow, 1987). Antiferromagnetic (AFM) order was found in the off-stoichiometric Ni_2MnZ alloy, in which the Mn atoms strongly prefer to occupy the 4a positions, and the excess Mn atoms occupy the 4b positions (Brown et al., 2006). The Mn atoms in the 4a site have ferromagnetic interaction, but in the 4b sites are coupled antiferromagnetically to the surrounding Mn atoms in the regular Mn sites (Krenke et al., 2005b). It is also true in both martensitic and austenitic states of the $Ni_{50}Mn_{35}In_{15}$ alloy (Bhobe et al., 2008). It means that excess Mn will enhance AFM interaction and result in weakness of ΔM when the alloy undergoes a magneto-structural transition from the paramagnetic martensitic state to the ferromagnetic austenitic state. The previous studies suggested that Co substitution in bulk $Ni_{43}Mn_{46-x}Co_xSn_{11}$ (Gao et al., 2009; Han et al., 2010) and $Ni_{42.7}Mn_{40.8}Co_{5.2}Sn_{11.3}$ ribbons (Ma et al., 2011) induced the Mn moments to align in a ferromagnetic order and enhance magnetization in the austenitic phase. It was also pointed out that the addition of Co in $Ni_{43}Mn_{46-x}Co_xSn_{11}$ alloys enhanced notably ΔM across MT, because magnetization of austenitic phase was significantly increased while that of martensitic state remained almost unchanged (Gao et al., 2009). The large MCE originating mainly from this large ΔM makes Ni–Mn–Co–Sn alloys potential refrigerants (Gao et al., 2009; Han et al., 2010). However, a lower Ni content or a higher Mn content in these alloys may enhance antiferromagnetic interaction, resulting in lower MCE.

In this work, the authors investigate the effect of Co substitution for Mn in higher Ni content Heusler alloys

[a]Author to whom correspondence should be addressed. Electronic mail: junqinli@szu.edu.cn

$Ni_{50}Mn_{35-x}Co_xSn_{15}$ on the martensitic transformation and MCE.

II. EXPERIMENTAL

The polycrystalline $Ni_{50}Mn_{35-x}Co_xSn_{15}$ alloys with $x = 0$, 1.0, 1.5, 2.0, and 3.0 were prepared by arc melting using a non-consumable tungsten electrode and a water-cooled copper tray in an atmosphere of pure argon. The alloys, each 6 g in total weight, were prepared using Ni, Mn, Co, and Sn with purity of 99.9 wt% as raw materials. The alloys were re-melted thrice to ensure homogeneity. The weight loss was measured from the weight before and after arc melting for each alloy button. The excess 3 wt% Mn was added to the alloy to compensate for evaporation of Mn during melting. Then, the alloy buttons were sealed in evacuated quartz tubes and annealed at 1173 K for 48 h, followed by quenching in liquid nitrogen. The sample was polished and etched using the solution of HNO_3:alcohol in the ratio 5:100, for the scanning electron microscope (SEM) observation and energy dispersive spectrum (EDS) analysis performed in a SU-70 scanning electron microscopy. X-ray powder diffraction (XRD) data were collected using a Bruker-axs D8 superspeed 18 kW diffractometer with $CuK\alpha$ radiation. The phase transformation temperatures and latent heat were analyzed by a TAQ200 differential scanning calorimeter (DSC) with a heating and cooling rate of 5 K min^{-1}. The temperature dependence and field dependence of magnetization were measured using a vibrating sample magnetometer (VSM). The thermomagnetic curves were recorded in an applied field of 0.1 T and the isothermal magnetization curves were measured in magnetic fields of 0–1.5 T.

III. RESULTS AND DISCUSSION

A. Structure and phase transition

XRD patterns of the $Ni_{50}Mn_{35-x}Co_xSn_{15}$ alloys with $x = 0$, 1.0, 1.5, 2.0, and 3.0 at room temperature, shown in Figure 1, indicate that all alloys are austenitic phases with the Heusler $L2_1$-type structure. The unit-cell parameters of the samples, obtained by Rietveld refinement method using Topas 3.0 software, were listed in Table I. One can see that the unit-cell parameters for the samples, except for the sample with $x = 3.0$, decrease with increasing Co content, due to the Co atom substitution for Mn atom in the structure. The empirical atomic radius (r_e) (Slater, 1964) of Co atom (1.35 Å) is smaller than that of Mn (1.40 Å) and Sn (1.45 Å) atoms but equal to that of Ni atom (1.35 Å). The Co and Mn are both transition elements, and the r_e of Co is closer to that of Mn than that of Sn. On the other hand, if we consider the calculated atomic radius (Clementi *et al.*, 1967) (r_c), the r_c of Co (1.52 Å) is larger than that of Ni (1.49 Å) and Sn (1.45 Å), and smaller than that of Mn (1.61 Å). Hence, it is preferred to substitute the Co for Mn not Ni or Sn. A second phase in the sample with $x = 3.0$ is observed from the shoulder at $2\theta = 43.04°$ and the diffraction peak at 73.85°, which is also confirmed by the SEM observation. The two peaks can be indexed as (011) and (112) with an NiMn-type structure (space group: $I4/mmm$). The presence of two crystalline phases is clearly observed in the SEM image, labeled with
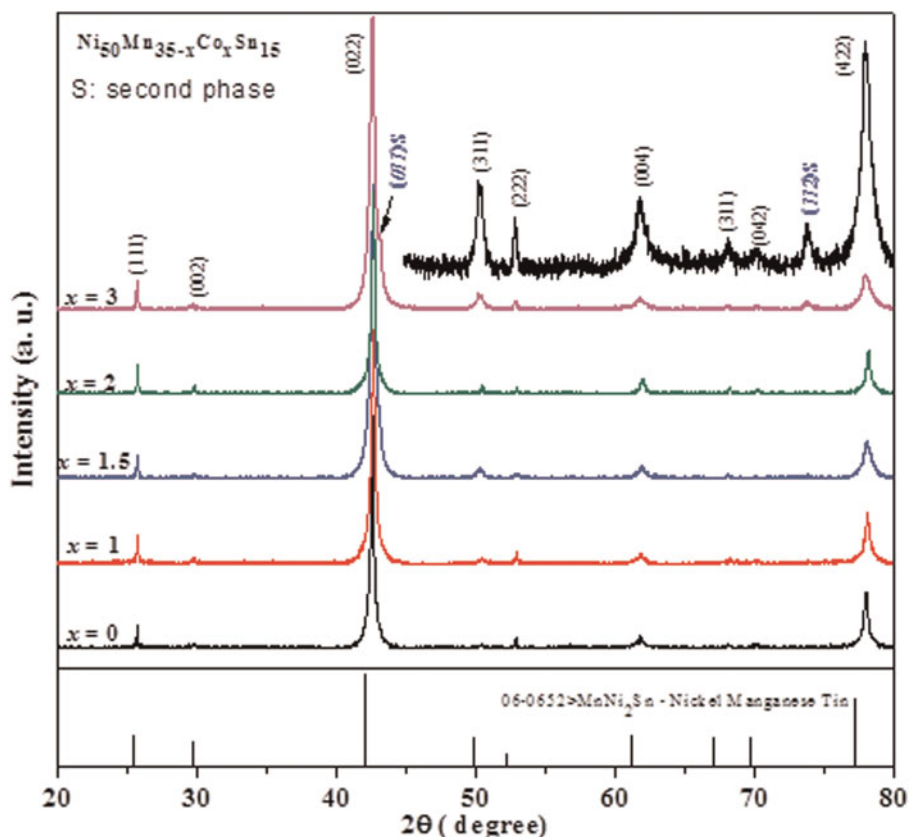

Figure 1. XRD patterns of $Ni_{50}Mn_{35-x}Co_xSn_{15}$ alloys with $x = 0$, 1, 1.5, 2, and 3. The label "06-0652 > $MnNi_2Sn$" is the ICDD powder diffraction file for Ni_2MnSn austenitic phase. An enlarged pattern for $x = 3$ is presented above.

TABLE I. Magnetic transformation temperatures, valence electron concentration (e/a), thermal hysteresis (ΔT), and lattice parameters a of austenitic phase for $Ni_{50}Mn_{35-x}Co_xSn_{15}$ (x = 0, 1, 1.5, 2 and 3) alloys.

X	M–T (K)			DSC (K)						e/a	Unit-cell parameter a (Å)
	A_s	A_f	T_c^A	A_s	A_f	M_s	M_f	ΔT	T_c^A		
0	185	205	324	–	–	–	–	–	322	8.05	6.001(1)
1.0	203	226	320	205	225	196	–	29	318	8.07	5.993(1)
1.5	240	259	310	242	261	235	216	27	309	8.08	5.990(1)
2.0	245	270	304	243	271	252	224	19	302	8.09	5.988(1)
3.0	–	–	323	–	–	–	–	–	323	8.02	6.001(1)

A and B in Figure 2. The EDX results show that the chemical composition is 50.1% Ni, 30.5% Mn, 17.3% Sn, and 2.1% Co in atomic percent for the A phase, and 59% Ni, 32.5% Mn, 2.5% Sn, and 6% Co for the B phase. The chemical formulas are $Ni_{50.1}Mn_{30.5}Sn_{17.3}Co_{2.1}$ and $Ni_{59}Mn_{32.5}Sn_{2.5}Co_6$, respectively. It is in good agreement with the reported decomposition of $Ni_{50}Mn_{50-x}Sn_x$ into $Ni_{50}Mn_{30}Sn_{20}$ and $Ni_{54}Mn_{45}Sn$ after 4 weeks annealing at 1223 K (Yuhasz *et al.*, 2009). As the chemical composition of $Ni_{59}Mn_{32.5}Sn_{2.5}Co_6$ is closer to that of NiMn, the alloy should be crystallized in the NiMn-type structure and $Ni_{50.1}Mn_{30.5}Sn_{17.3}Co_{2.1}$ as the $L2_1$ austenite phase. The decomposition occurred in the sample with x = 3.0 annealed at 1173 K for only 48 h in this work, implying that the doping of Co led to decomposition at a lower temperature and a shorter annealing time.

The DSC cooling and heating curves between 200 and 420 K for the $Ni_{50}Mn_{35-x}Co_xSn_{15}$ alloys are shown in Figure 3. The sharp exothermic and endothermic peaks, corresponding to the reverse martensitic reverse transformation and direct martensitic transformation, show the martensitic start (M_s) and finish (M_f) temperatures, the austenitic start (A_s) and finish (A_f) temperatures, and the Curie temperature (T_C^A) of the austenitic phase. The results obtained from these DSC curves are listed in Table I. Only the endothermic peak of austenitic transition was observed for the sample with x = 1.0, while no other peaks of martensitic or austenitic transformation for the sample with x = 0 were detectable. The martensitic transformation was not observed by DSC for the sample with x = 3.0. Generally, the thermal hysteresis is regarded as a typical feature of the martensitic transformation due to the first-order nature of the transition (Ortin and Delaey, 2002). The thermal hysteresis around T_M is about 20–30 K for $Ni_{50}Mn_{35-x}Co_xSn_{15}$ alloys.

Figure 4 shows the temperature dependence of the magnetization (M–T curves) for the $Ni_{50}Mn_{35-x}Co_xSn_{15}$ compounds with x = 0, 1.0, 1.5, 2.0, and 3.0 in an applied field of 0.1 T. The MT is not found in the M–T curve for the sample with x = 3.0 till 80 K, which may be due to the decomposition of this sample mentioned above. The same phenomenon had also been reported in $Ni_{50-x}Co_xMn_{39}Sb_{11}$ alloy for x = 11

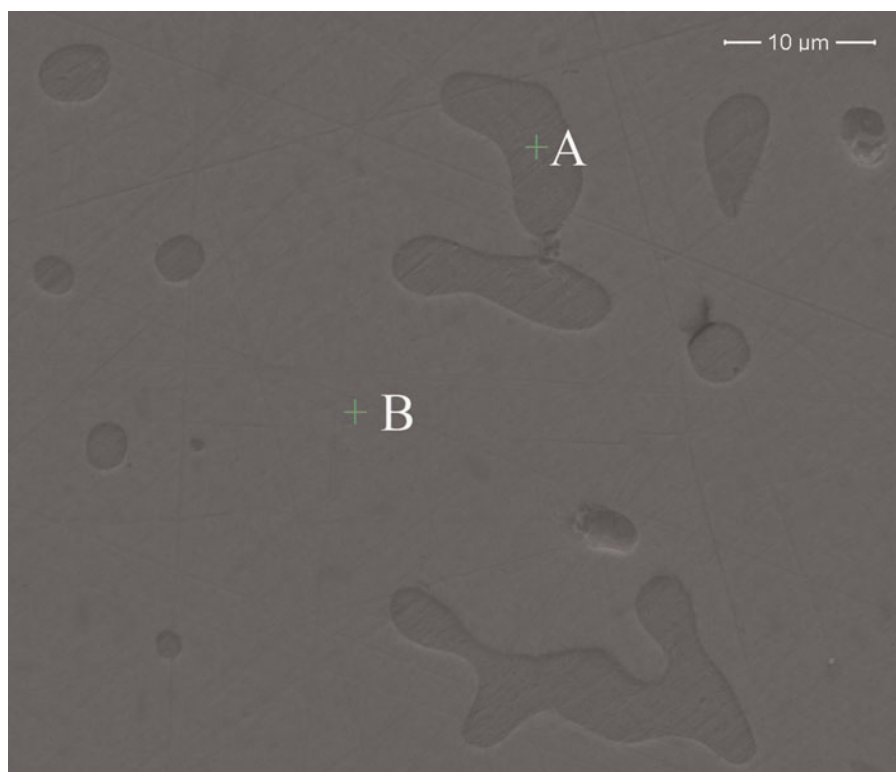Figure 2. SEM image of $Ni_{50}Mn_{32}Co_3Sn_{15}$ shows the presence of two phases. EDX spectroscopy indicates that the compositions of A and B are $Ni_{59}Mn_{32.5}Sn_{2.5}Co_6$ and $Ni_{50.1}Mn_{30.5}Sn_{17.3}Co_{2.1}$, respectively.
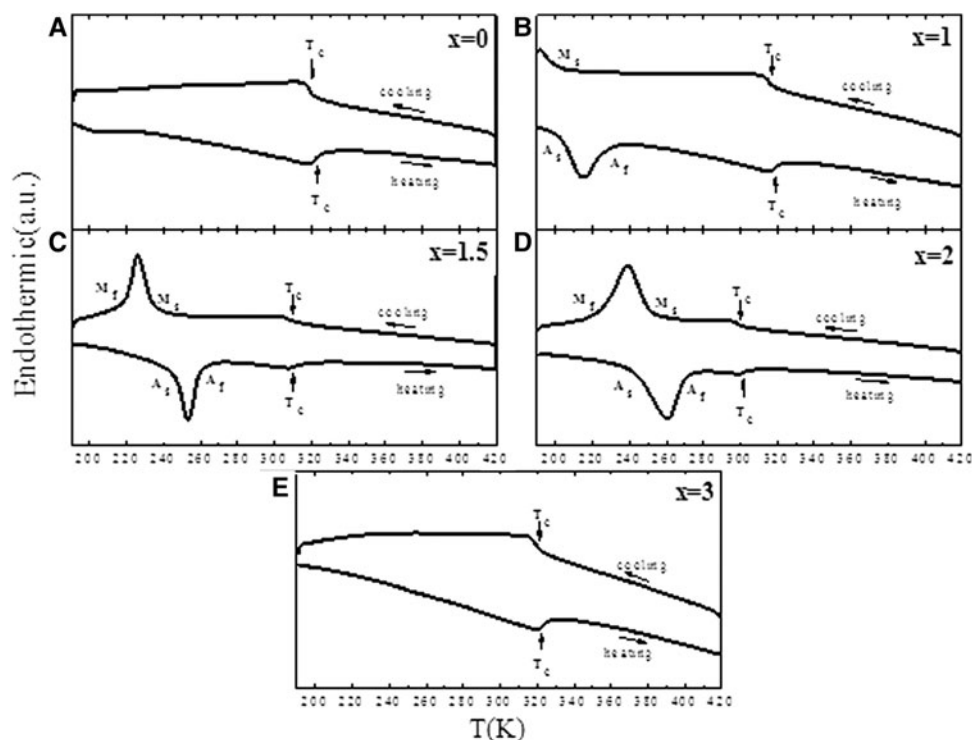
Figure 3. DSC curves for the $Ni_{50}Mn_{35-x}Co_xSn_{15}$ alloys with $x = 0$ (a), 1 (b), 1.5 (c), 2 (d), and 3 (e) on both heating and cooling modes.

due to the suppression of the martensitic phase by Co doping (Han *et al.*, 2008). Krenke *et al.* (2007) calculated the density of states (DOS) for the $L2_1$, $L1_0$, and 5M modulated structures for Ni_2MnGa, and pointed out that the modulated martensitic states are metastable from the DOS. It was also reported that an MT occurs in the alloys having a critical value of the unit-cell parameter $a \approx 6$ Å or less in the austenitic state for the NiMn-based Heusler alloys (Planes *et al.*, 2009). The unit-cell parameter of $Ni_{50.1}Mn_{30.5}Sn_{17.3}Co_{2.1}$ alloy is about $a = 6.001$ Å, which may attribute to the disappearance of MT for the alloy with $x = 3.0$. However, the unit-cell parameter a for the sample with $x = 0$ is also equal to 6.001 Å, but the MT of this sample occurred because the valence electron concentration e/a is also a critical factor influencing the characteristics of MT. It has been well established that the compositional dependence of temperature of MT (T_M) and T_C for martensitic and austenitic phases are closely related to e/a. The e/a-dependence of T_M has been found to increase monotonously (Planes *et al.*, 2009). The valence electron concentration e/a of $Ni_{50.1}Mn_{30.5}Sn_{17.3}Co_{2.1}$ is 8.02. According to Planes *et al.* (2009), the temperature of MT for $Ni_{50.1}Mn_{30.5}Sn_{17.3}Co_{2.1}$ will expect to be about 150 K, but actually not occur. It is maybe the affection of lattice parameter or the existence of the second phase.

The A_s, A_f and T_C^A estimated from the M–T curves are also listed in Table I. The results obtained from the DSC analysis agree well with those obtained from M–T measurements. With increasing temperature, the M–T curves of $Ni_{50}Mn_{35-x}Co_xSn_{15}$ compounds, except for the sample with $x = 3.0$, show a slightly tilted platform first and then climb sharply at A_s with reverse magnetic transformation accompanied with MT. The A_s determined from Figure 2 are 185, 203, 240, and 245 K for the samples with $x = 0$, 1.0, 1.5, and 2.0, respectively. On further increase in temperature, the austenitic undergoes a ferromagnetic transition from the FM state to the PM state. The M–T curves for the samples, except for $x = 3.0$, show clearly that the austenitic transformation temperatures are increasing but T_C^A is decreasing with increasing Co content, because the valence electron concentration e/a of the alloy is increased with increasing Co content.

For the samples with $x = 1.0$, 1.5, and 2.0, maximum magnetizations of the austenitic state increase from 24 to 28 Am^2 kg^{-1}. However, the ΔM does not increase with increasing Co content because magnetizations of the martensitic state increase too. In the earlier reports, it was suggested that Co substitution helps the Mn moments align in a ferromagnetic ordering, giving rise to the magnetization in the austenitic phase (Yu *et al.*, 2007; Kainuma *et al.*, 2008; Ma *et al.*,
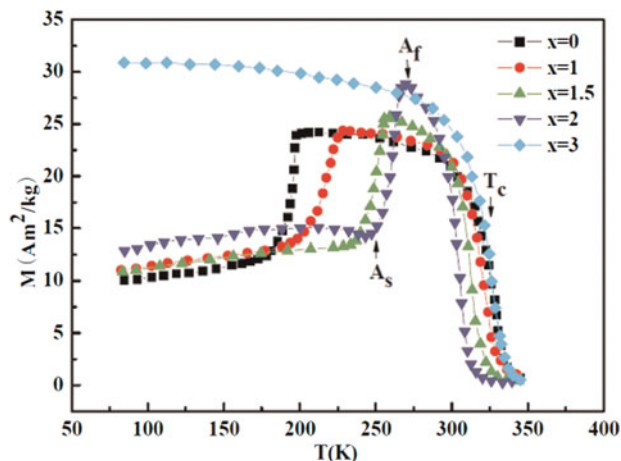

Figure 4. Temperature-dependent magnetization (M–T) curves for $Ni_{50}Mn_{35-x}Co_xSn_{15}$ alloys in a field of 0.1 T.

2008; Han *et al.*, 2010). The calculated result of Co-doped Mn_2NiGa with the first principle confirmed that Co acts as a ferromagnetic activator, and leads to ferromagnetic alignment of Mn moments in the austenitic phase (Ma *et al.*, 2008). The exchange coupling is suggested to be a competition between the spin polarization of transportation electrons among localized Mn moments and the s–p hybridizing effect induced by Co. According to the calculation results (Ma *et al.*, 2008), the original two Mn sites become three sites when the Co atom enters the Mn_2NiSn-type lattice because the embedded Co atom breaks the crystallographic symmetry. Therefore, a similar mechanism may account for this system.

B. Magnetocaloric effect

The isothermal magnetization (*M–H*) curves for $Ni_{50}Mn_{35-x}Co_xSn_{15}$ alloys have been measured near T_M. The magnetization loop in both increasing and decreasing fields is presented in Figure 5. It shows the *M–H* curves for the alloy $Ni_{50}Mn_{33.5}Co_{1.5}Sn_{15}$ measured at various temperatures around T_M in the magnetic field range of 0–1.5 T. Hysteresis losses are detected. The increment in temperature is 2 K with increasing temperature mode. The curves below 240 K and above 259 K reveal low magnetization in the martensitic phase but high magnetization in the austenitic phase, respectively. At temperatures between 245 and 255 K, the metamagnetic behavior characterized by magnetic hysteresis has been observed, which confirms a reversible martensitic transformation that can be induced by applying a magnetic field. Using the Maxwell relation $(\partial S / \partial H)_T = (\partial M / \partial T)_H$, the magnetic entropy changes can be calculated as.

$$\Delta S_M(T, H) = S_M(T, H) - S_M(T, 0)$$
$$= \int_0^H \left(\frac{\partial S_M}{\partial H} \right)_T dH = \int_0^H \left(\frac{\partial M}{\partial T} \right)_H dH \quad (1)$$

The sign of ΔS_M is determined by the sign of $\partial M / \partial T$, as shown in Eq. (1). The majority of the reported ΔS_M values of Ni–Mn–Ga and other ferromagnetic systems exhibiting first-order phase transition are calculated using Eq. (1). Based on this common practice, the ΔS_M (*T*, *H*) of
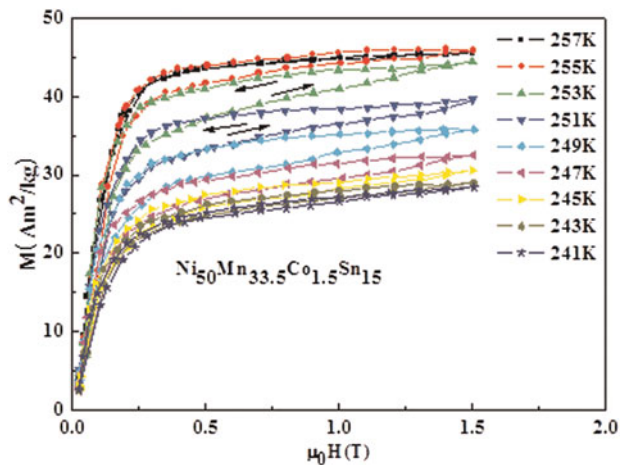

Figure 5. Isothermal magnetization loops (*M–H* curves) for the alloy of $Ni_{50}Mn_{33.5}Co_{1.5}Sn_{15}$ measured at various temperatures around T_M in a magnetic field range of 0–1.5 T.

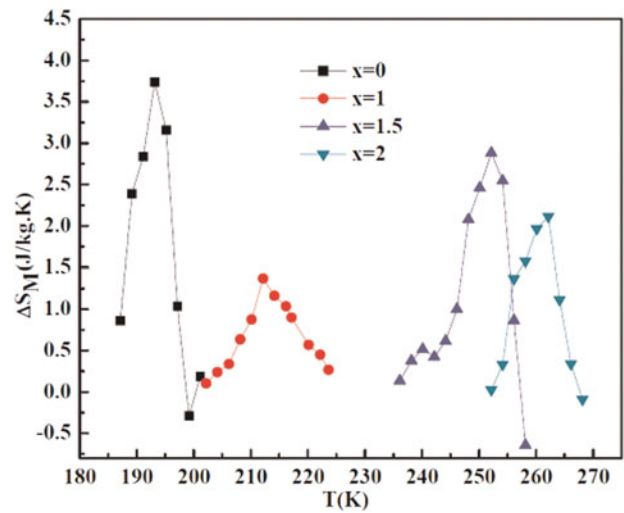Figure 6. Magnetic entropy change ΔS_M of $Ni_{50}Mn_{35-x}Co_xSn_{15}$ alloys in a magnetic field range of 0–1.5 T.

$Ni_{50}Mn_{35-x}Co_xSn_{15}$ alloys are shown in Figure 6, which is evaluated with a magnetic field change of 1.5 T. Peaks can be observed near T_M and the calculated maximum values of ΔS_M are 3.73, 1.37, 2.88, and 2.11 $J\,kg^{-1}\,K^{-1}$ for $x = 0$, 1.0, 1.5, and 2.0, respectively. The maximum magnetic entropy change of 3.73 $J\,kg^{-1}\,K^{-1}$ is obtained in $Ni_{50}Mn_{35}Sn_{15}$ alloy with a magnetic field change of 1.5 T at about 193 K, which is comparable with 5 $J\,kg^{-1}\,K^{-1}$ in a field of 2 T and 2.2 $J\,kg^{-1}\,K^{-1}$ in a field of 1 T for $Ni_{50}Mn_{35}Sn_{15}$ (Krenke *et al.*, 2005a), whereas the effect of Co addition on MCE is not obvious in this work, Co addition promotes T_M from 196 to 252 K. As a result, Co-doped Ni–Mn-based Heusler alloys possess potential applications as magnetic refrigerants at an appropriate temperature.

VI. CONCLUSION

In summary, the effect of Co substitution on the martensitic transformation and MCE of $Ni_{50}Mn_{35}Sn_{15}$ alloy has been investigated. $Ni_{50}Mn_{35-x}Co_xSn_{15}$ ($x = 0$, 1, 1.5, 2, and 3) alloys have the Heusler $L2_1$-type structure at room temperature. For the sample with $x = 3.0$, it decomposes into two phases with the chemical compositions of $Ni_{50.1}Mn_{30.5}Sn_{17.3}Co_{2.1}$ and $Ni_{59}Mn_{32.5}Sn_{2.5}Co_6$. With an increase of the Co content from 0 to 2.0, the martensitic transformation temperature T_M increases from 185 to 245 K. This agrees with the rule of *e/a*-dependence of T_M. The maximum magnetic entropy changes ΔS_M of 3.73, 1.37, 2.88, and 2.11 J $kg^{-1}\,K^{-1}$ are obtained for the samples $x = 0$, 1.0, 1.5, and 2.0, respectively, near their martensitic transformation temperatures in a magnetic field change of 1.5 T. Co doping promotes T_M to an appropriate temperature range, which may have potential applications as magnetic refrigerants near room temperature.

Bhobe, P. A., Priolkar, K. R., and Nigam, A. K. (**2008**). "Anomalous magnetic properties in $Ni_{50}Mn_{35}In_{15}$," J. Phys. D. Appl. Phys. **41**, 235006.

Brown, P. J., Gandy, A. P., Ishida, K., Kainuma, R., Kanomata, T., Neumann, K. U., Oikawa, K., Ouladdiaf, B., and Ziebeck, K. R. A. (**2006**). "The magnetic and structural properties of the magnetic shape memory compound $Ni_2Mn_{1.44}Sn_{0.56}$," J. Phys., Condens. Matter, (UK) **18**, 2249–2259.

Clementi, E., Raimondi, D. L., and Reinhardt, W. P. (**1967**). "Atomic screening constants from Scf functions. II. Atoms with 37 to 86 electrons," J. Chem. Phys. **47**, 1300–1308.

Gao, B., Hu, F. X., Shen, J., Wang, J., Sun, J. R., and Shen, B. G. (**2009**). "Field-induced structural transition and the related magnetic entropy change in $Ni_{43}Mn_{43}Co_3Sn_{11}$ alloy," J. Magn. Magn. Mater. **321**, 2571–2574.

Han, Z. D., Wang, D. H., Zhang, C. L., Xuan, H. C., Zhang, J. R., Gu, B. X., and Du, Y. W. (**2008**). "The phase transitions, magnetocaloric effect, and magnetoresistance in Co doped Ni-Mn-Sb ferromagnetic shape memory alloys," J. Appl. Phys. **104**, 053906.

Han, Z., Wang, D., Qian, B., Feng, J., Jiang, X., and Du, Y. (**2010**). "Phase transitions, magnetocaloric effect and magnetoresistance in Ni–Co–Mn–Sn ferromagnetic shape memory alloy," Jpn. J. Appl. Phys. **49**, 010211.

Helmholdt, R. B. and Buschow, K. H. J. (**1987**). "Crystallographic and magnetic structure of Ni_2MnSn and $NiMn_2Sn$," J. Less-Common Met. **128**, 167–171.

Hu, F. X., Shen, B. G., Sun, J. R., Cheng, Z. H., Rao, G. H., and Zhang, X. X. (**2001**). "Influence of negative lattice expansion and metamagnetic transition on magnetic entropy change in the compound $LaFe_{11.4}Si_{1.6}$," Appl. Phys. Lett. **78**, 3675–3677.

Kainuma, R., Imano, Y., Ito, W., Sutou, Y., Morito, H., Okamoto, S., Kitakami, O., Oikawa, K., Fujita, A., Kanomata, T., and Ishida, K. (**2006**). "Magnetic-field-induced shape recovery by reverse phase transformation," Nature **439**, 957–960.

Kainuma, R., Ito, W., Umetsu, R. Y., Oikawa, K., and Ishida, K. (**2008**). "Magnetic field-induced reverse transformation in B2-type nicomnal shape memory alloys," Appl. Phys. Lett. **93**, 091906.

Krenke, T., Duman, E., Acet, M., Wassermann, E. F., Moya, X., Manosa, L., and Planes, A. (**2005a**). "Inverse magnetocaloric effect in ferromagnetic Ni-Mn-Sn alloys," Nat. Mater. **4**, 450–454.

Krenke, T., Acet, M., Wassermann, E. F., Moya, X., Manosa, L., and Planes, A. (**2005b**). "Martensitic transitions and the nature of ferromagnetism in the austenitic and martensitic states of Ni-Mn-Sn alloys," Phys. Rev. B **72**, 014412.

Krenke, T., Moya, X., Aksoy, S., Acet, M., Entel, P., Manosa, L., Planes, A., Elerman, Y., Yucel, A., and Wassermann, E. F. (**2007**). "Electronic aspects of the martensitic transition in Ni-Mn based Heusler alloys," J. Magn. Magn. Mater. **310**, 2788–2789.

Kuhrt, Ch., Schittny, Th. and Bärner, K. (**1985**). "Magnetic B–T phase diagram of anion substituted MnAs. magnetocaloric experiments," Phys. Status Solidi A (Germany). **91**, 105–113.

Ma, L., Zhang, H. W., Yu, S. Y., Zhu, Z. Y., Chen, J. L., Wu, G. H., Liu, H. Y., Qu, J. P., and Li, Y. X. (**2008**). "Magnetic-field-induced martensitic transformation in MnNiGa:Co alloys," Appl. Phys. Lett. **92**, 032509.

Ma, S. C., Cao, Q. Q., Xuan, H. C., Zhang, C. L., Shen, L. J., Wang, D. H., and Du, Y. W. (**2011**). "Magnetic and magnetocaloric properties in Melt-Spun and annealed $Ni_{42.7}Mn_{40.8}Co_{5.2}Sn_{11.3}$ ribbons," J. Alloy. Compd. **509**, 1111–1114.

Ortin, J., and Delaey, L. (**2002**). "Hysteresis in shape-memory alloys," Int. J. Nonlinear Mech. **37**, 1275–1281.

Pasquale, M., Sasso, C., Lewis, L., Giudici, L., Lograsso, T., and Schlagel, D. (**2005**). "Magnetostructural transition and magnetocaloric effect in $Ni_{55}Mn_{20}Ga_{25}$ single crystals," Phys. Rev. B **72**, 094435.

Pecharsky, V. K. and Gschneidner, K. A. (**1997**). "Giant magnetocaloric effect in $Gd_5(Si_2Ge_2)$," Phys. Rev. Lett. **78**, 4494–4497.

Planes, A., Manosa, L., and Acet, M. (**2009**). "Magnetocaloric effect and its relation to shape-memory properties in ferromagnetic Heusler alloys," J. Phys., Condens. Matter, (UK) **21**, 233201.

Slater, J. C. (**1964**). "Atomic radii in crystals," J. Chem. Phys. **41**, 3199–3205.

Tegus, O., Bruck, E., Buschow, K. H. J., and de Boer, F. R. (**2002**). "Transition-metal-based magnetic refrigerants for room-temperature applications," Nature **415**, 150–152.

Wada, H. and Tanabe, Y. (**2001**). "Giant magnetocaloric effect of $MnAs_{1-x}Sb_x$," Appl. Phys. Lett. **79**, 3302–3304.

Yu, S. Y., Cao, Z. X., Ma, L., Liu, G. D., Chen, J. L., Wu, G. H., Zhang, B., and Zhang, X. X. (**2007**). "Realization of magnetic field-induced reversible martensitic transformation in nicomnga alloys," Appl. Phys. Lett. **91**, 102507.

Yuhasz, W. M., Schlagel, D. L., Xing, Q., Dennis, K. W., McCallum, R. W., and Lograsso, T. A. (**2009**). "Influence of annealing and phase decomposition on the magnetostructural transitions in $Ni_{50}Mn_{39}Sn_{11}$," J. Appl. Phys. **105**, 07A921.

Zhang, C. L., Wang, D. H., Cao, Q. Q., Han, Z. D., Xuan, H. C., and Du, Y. W. (**2008**). "Magnetostructural phase transition and magnetocaloric effect in off-stoichiometric $Mn_{1.9-x}Ni_xGe$ Alloys," Appl. Phys. Lett. **93**, 122505.

Zhang, X. X., Tejada, J., Xin, Y., Sun, G. F., Wong, K. W., and Bohigas, X. (**1996**). "Magnetocaloric effect in $La_{0.67}Ca_{0.33}MnO_{delta}$ and $La_{0.60}Y_{0.07}Ca_{0.33}MnO_{delta}$ bulk materials," Appl. Phys. Lett. **69**, 3596–3598.